EXTENDED LOCAL BINARY PATTERNS-BASED POLARIMETRIC SYNTHETIC APERTURE RADAR IMAGE CLASSIFICATION

Andreia Valentina MICLEA-CECALACA, Ioana Ilea, Romulus TEREBES
Communications Department, Technical University of Cluj-Napoca, Cluj-Napoca, Romania
Andreia.Miclea@com.utcluj.ro, Ioana.Ilea@com.utcluj.ro, Romulus.Terebes@com.utcluj.ro

Abstract: Polarimetric Synthetic Aperture Radar (PolSAR) imaging has emerged as a powerful tool for remote sensing applications, providing valuable insights into the physical properties of observed targets. Among various methods employed for PolSAR image analysis, the Local Binary Patterns (LBP) algorithm has gained significant attention due to its robustness and efficiency in texture classification tasks. However, conventional LBP approaches often encounter challenges in capturing complex texture patterns and preserving discriminative information inherent in PolSAR images. In this paper, we propose an integration of the classical Extended Local Binary Patterns (ELBP) method into a framework specifically designed for PolSAR image analysis. The ELBP method integrates advanced feature extraction techniques based on multiresolution analysis to enhance the discriminative power of texture descriptors. By exploiting the polarimetric information embedded in PolSAR images, the ELBP method effectively captures intricate texture characteristics while preserving spatial context. Comparative analyses against state-of-the-art texture analysis techniques demonstrate the efficiency of the ELBP method in terms of classification accuracy.

Keywords: *ELBP, PolSAR imaging, polarization, SVM*

I. INTRODUCTION

Radar images obtained with a Synthetic Aperture Radar (SAR) system that possesses polarimetric capabilities are referred to as polarimetric SAR images (PolSAR). Polarimetric SAR systems can emit and receive radar signals in multiple polarization states concurrently, in contrast to conventional SAR systems that can only transmit and receive radar signals in a single polarization, usually horizontal or vertical direction. The corresponding polarization states, which include horizontal (HH), vertical (VV), and cross-polarized (HV or VH) images, represent the rich data gathered from the scene's scattering properties [1].

Different parameters, in terms of type and number, can be derived from the scene under observation based on the organization of information in the polarimetric SAR images. These parameters may include the vegetation characteristics, or the specific target classification, the roughness of the observed area or the moisture content. The polarimetric SAR images have been used in different fields, such as military reconnaissance, forestry, agriculture, disaster relief or environmental monitoring.

The PolSAR sensors are very suitable for continuous monitoring of a scene, the polarimetric systems being capable of collecting the information regardless of the weather conditions (clouds, fog) or the period of the day (night or daytime). Also, the polarimetric SAR signals have the ability to penetrate through vegetation, providing information about the underlying terrain or objects obscured by foliage. This type of collected information, providing richer data in terms of scattering properties allows for advanced analysis techniques for material discrimination in a scene [1].

Due to its abundant information, different types of features can be extracted from the PolSAR images. These features are derived from complex data and are used for various purposes such as classification, target detection, and parameter estimation. Statistical descriptors and texture features are some of the popular feature extraction methods applied on polarimetric data, as presented in [2], [3] and [4]. Features derived from statistical analysis of polarimetric data include mean, variance, covariance, correlation, entropy, while the texture features can be derived from the gray-level co-occurrence matrices (GLCM), wavelet transforms, or Local Binary Patterns (LBP). The mentioned methods can extract the features from the PolSAR data that can be used independently or combined into a single feature vector. In order to validate the efficiency of the extracted features, machine learning algorithms are often employed, typically the Support Vector Machines (SVM) classifier.

The GLCM and LBP methods are used to extract valuable information from a rich data set. Due to the capability of providing information regarding the texture properties as contrast, correlation, energy or homogeneity, the GLCM [5] method has proven to be sensitive to the spatial arrangement of backscatter values in PolSAR images, allowing for the characterization of textural features, as presented in [6]. In paper [6], a fused feature vector was proposed, based on the most common texture information extraction techniques, the GLCM and LBP approaches, which resulted in good accuracy, for the SVM classifier.

The structure of the paper is as follows: in Section II, we introduce our approach within the framework of polarimetric SAR remote sensing. Section III is devoted to experimental validation, where we present the classification results on real, respectively simulated PolSAR images, where varying ages of maritime pine forest is observed, with different acquisition resolutions. Lastly, the concluding section summarizes our findings and outlines potential avenues for future research.

Manuscript received March 29, 2024; revised May 21, 2024

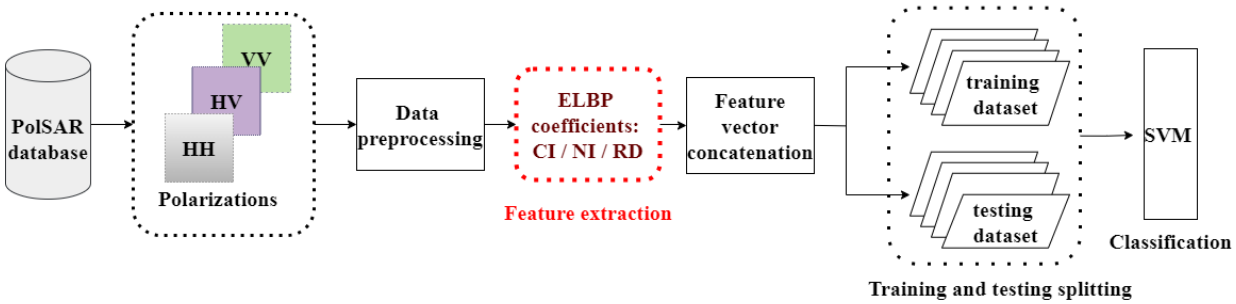

Figure 1. Polarimetric SAR image classification framework.

II. PROPOSED METHOD

The proposed machine learning methodology for this study, for polarimetric SAR image classification is depicted in Fig. 1, where from the PolSAR database, the three polarizations are used, HH, HV and VV, to evaluate the efficiency of the feature extraction ELBP method. In this paper, on each individual polarized image, a preprocessing stage is applied, followed by the ELBP feature extraction method where specific features are extracted. Then those features are concatenated into a single feature vector, as in [7], then fed to a SVM classifier.

A. PolSAR data acquisition and preprocessing

In polarimetric synthetic aperture radar imaging, polarization refers to the orientation of the transmitted and received radar waves with respect to the Earth's surface, in which the systems utilize antennas capable of transmitting and receiving signals in different polarizations. During data acquisition, the radar system emits electromagnetic waves towards the Earth's surface which scatter in various directions. The radar system then receives the backscattered signals that carry the information about the surface characteristics of the observed area.

In PolSAR systems, the received signals are recorded in the form of complex-valued matrices, where each element represents the amplitude and phase of the signal in a specific polarization channel. Thus, a scattering matrix (S) outlines the manner in which a target scatters after coming into contact with an electromagnetic pulse, by integrating into the matrix the emitted and backscattered signals' horizontal and vertical polarization phases. When electromagnetic waves from a source interact with surface-placed scatterers, backscattered electromagnetic waves are produced. These backscattered waves are determined by the physical characteristics of the objects in the acquired scene, such as their spatial dimensions or the type of the material, within a specified range in the direction of the flying path, known as azimuth in SAR terminology.

A mathematical expression can be used to describe the relationship between the incident, denoted by E_h^i and E_v^i, for the horizontal and vertical directions, and the scattered electromagnetic waves, E_h^s and E_h^s, for a given wavenumber $k = 2\pi/\lambda$ and a certain distance r between the target and the receiver:

$$\begin{bmatrix} E_h^s \\ E_v^s \end{bmatrix} = \frac{e^{-jkr}}{r} \begin{bmatrix} S_{hh} & S_{hv} \\ S_{vh} & S_{vv} \end{bmatrix} \begin{bmatrix} E_h^i \\ E_v^i \end{bmatrix} = S \begin{bmatrix} E_h^i \\ E_v^i \end{bmatrix} \quad (1)$$

The scattering matrix (S) from equation (1) quantifies the scattering attributes of the fixed targets and includes complex coefficients. Two different receiving antennas are used to measure the associated coefficients in order to detect the vertical and horizontal reflected polarized waves, respectively [8]. The diagonal coefficients are assumed to be equal if the sender and the recipient are in the same location, indicating that the information contained in the HV and VH polarization is the same.

By combining information from different polarization states, PolSAR imaging can provide a richer understanding of the scattering properties and surface characteristics of the observed area. In this situation the analysis of multiple polarization channels allows for more accurate classification of the data.

Our method transforms the diagonal, respectively the vertical scattering coefficients logarithmically as illustrated in the following equation, for HH, VH and VV [6]:

$$\begin{aligned} I_{hh} &= 10log\,(S_{hh} \cdot S_{hh}^*) \\ &= 10log[Re^2(S_{hh}) + Im^2(S_{hh})] \\ I_{hv} &= 10\log\,(S_{hv} \cdot S_{hv}^*) \\ &= 10log[Re^2(S_{hv}) + Im^2(S_{hv})] \\ I_{vv} &= 10\log\,(S_{vv} \cdot S_{vv}^*) \\ &= 10log[Re^2(S_{vv}) + Im^2(S_{vv})] \end{aligned} \quad (2)$$

The logarithmic transformation from equation (2) is applied in the preprocessing stage from Fig. 1, for the three polarizations, to improve the data quality by transforming the multiplicative noise that characterize the PolSAR images into an additive noise.

B. Extended LBP feature extraction approach

The Local Binary Patterns [9] technique was used for PolSAR image processing due to the complex textures preset in this type of database as a result of radar wave interactions with many sorts of surfaces and materials. Because local patterns of intensity variations within the image are encoded, the LBP approach efficiently captures these textures. Based on the strong capability to extract information from any type of data that contains texture, the LBP method has evolved in new methods such as Extended ELBP [10] or SSELBP [11].

For the LBP method a binary set is constructed for a particular center pixel by comparing its gray value, denoted by t_c, to that of its neighbors, t_i. Then, the function $s(\cdot)$, attributes a value of 0 or 1, for each neighbor inside a specified area [9]:

$$s(t_i - t_c) = \begin{cases} 1, & if\ t_i - t_c \geq 0 \\ 0, & if\ t_i - t_c < 0. \end{cases} \quad (3)$$

A set of data points with uniform spacing within a circle with radius R is defined in order to determine which pixels are adjacent to the centered pixel. By placing P neighbors evenly around the circle of radius R, the LBP code is created:

$$LBP_{P,R}(t_c) = \sum_{i=0}^{P-1} s(t_i - t_c) \cdot 2^i. \quad (4)$$

Thus, the probability distribution of the 2^p LBP patterns can be used to describe a texture image. By varying the parameters (R, P), the LBP operator has been extended to multiscale analysis, allowing for any radius and number of pixels in the neighborhood.

However, the LBP method has some limitations due to the sensitivity of different patterns to the orientation of the image, which can limit their effectiveness in tasks where rotation invariance is crucial. To eliminate these issues a rotational invariant LBP was developed [9] by considering multiple rotations of the local neighborhood pattern and selecting the most representative pattern among them. By capturing texture information in a rotationally invariant manner, this variant of LBP enables more robust texture analysis in situations where the orientation of the image may vary:

$$LBP_{P,R}^{ri}(t_c) = \min\{ROR(LBP_{P,R}, i) \mid i = 0,1,2 \dots P-1\}, \quad (5)$$

where $ROR(\cdot)$ ensures that a step circular bit-wise right shift is performed on the $LBP_{P,R}$, in order to preserve only the patterns with rotationally unique codes. Based on the notion of uniform and non-uniform patterns, a grouping of those LBP codes is proposed in [9], where the uniform patterns are grouped in $p+1$ different rotation invariant patterns. Those groups are dependent on the $U(\cdot)$ function designed to count the bitwise transitions from the 0 bit to the 1 bit, respectively from the 1 bit to the 0 bit, to ensure that the corresponding categories of LBP codes represent rotational invariant uniform descriptors $LBP_{P,R}^{riu2}$:

$$LBP_{P,R}^{riu2}(t_c) = \begin{cases} \sum_{i}^{P-1} s(t_i - t_c), & if\ U(\sum_{i=0}^{P-1} s(t_i - t_c)) \le 2 \\ P+1, & otherwise. \end{cases} \quad (6)$$

The ELBP method is designed as the extension of the LBP concept by considering a wider range of pixel comparisons, leading to a richer representation of local texture patterns. The ELBP method uses three descriptors CI, NI, and RD capable of capturing more complex texture variations compared to traditional LBP by including additional neighboring pixels in the pattern encoding process [10]. The following equations represent the three descriptors determined for the ELBP method:

$$\mathrm{CI}(t_c^*) = s(t_c^* - \beta),$$
$$\mathrm{NI}_{R,P}(t_c^*) = \sum_{k=0}^{P-1} s\left(t_{R,P,n}^* - \beta_{R,P}\right) \cdot 2^n,$$
$$\mathrm{RD}_{R,R-1,P}(t_c^*) = \sum_{k=0}^{P-1} s\left(t_{R,P,n}^* - t_{R-1,P,n}^*\right) \cdot 2^n \quad (7)$$

In equation (7), for the CI descriptor, the t_c^* represents the central pixel, while β represents the average of the entire image. For the NI descriptor instead of averaging the gray value of the entire image, the operator creates the code by averaging the intensities of the surrounding pixels in a window size of $w_R \times w_R$ dimension, considering the local mean $\beta_{R,P}$ calculated in the local window. For the RD operator, the code is generated by comparing the brightness of pixels placed on a different radial direction, where the one radius has a smaller value than the other radius, both centered on the central pixel.

III. EXPERIMENTAL RESULTS

A. Datasets

For the experimental evaluation, a simulated and a real PolSAR image was used, containing maritime pine forest stands, with different ages. In order to determine the impact of the three descriptors on the classification accuracy for various polarizations, we tested the ELBP approach using a real L-band airborne PolSAR image similarly to [2] and [12] as shown in Fig. 2. During the ONERA RAMSES campaign in 2004, this data was taken above the French Nezer forest, representing maritime pine tree forests stands with 1 meter resolution. The data contains pine trees that range in age from 5 to 48 years, distributed in 62 forest stands, which were categorized by experts into four age groups: less than 10 years, between 10 and 20 years, between 21 and 30 years and more than 30 years [2].

In Fig. 2 a section of the real data is shown, for the 4 polarizations, HH, VH, HV and VV, for a patch in which the pine trees are 15 years old. Using the PolSARproSIM program [13], an aerial system operating in the L band was simulated in order to create simulated PolSAR images.

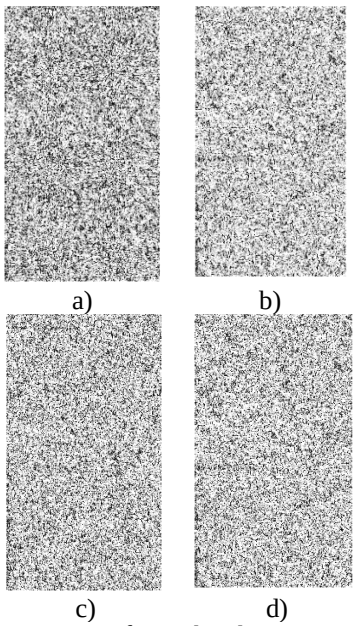

Figure 2. A segment of a real PolSAR image pine trees (1m resolution) having 15 years, for different polarizations, at: a) HH, b) HV, c) VV, d) VH

The incidence angle for the simulated dataset is fixed at 45°, with varying azimuth resolutions of 0.5, 1, 2, 3, and 5 meters. Using the same experimental approach as in [12], polarimetric SAR images representing pine tree forest stands aged between 5 and 32 years have been generated for every individual resolution, for the HH, HV, VH and VV polarizations similarly to the real PolSAR data. In Fig. 3 a simulated PolSAR image is illustrated with 1 meter resolution, for all four polarizations, similar to the real data, where the pine trees are 15 years old.

By analyzing Fig. 2 and Fig.3, we can observe that the information from the HV and VH polarization is similar. Based on this, for the experimental evaluation, we consider only the information from the HH, HV, respectively VV polarizations.

B. Implementation

The machine learning workflow with the SVM classifier shown in Fig. 1 was implemented using Matlab. With the SVM, a one-versus-one coding scheme and a linear kernel are used to train the data for the multiclass classification problem. The training dataset contains 50% polarized images from the PolSAR database, the remaining images being used for the testing data set. To provide mean accuracy values and standard deviations, we partitioned the training and testing sets 100 times. In order to test the performance of the ELBP method, the three descriptors were used only for the HH, HV and VV polarizations.

For the ELBP descriptors, the neighbors were set at $P = 8$, while the radii have taken different values of 2, 4, 6 and 8. For the experiments presented in this study, we use only the radii of 2, respectively 4, for the descriptors, due to the multiresolution analysis of the data, by concatenating the histograms from multiple resolutions in a single histogram, representing the feature vector used in classification [7]. For the experimental evaluation different combinations of descriptors were created as joint histograms using the mentioned radii. For the second part of the evaluation a Gaussian filtering stage is added, after the data preprocessing stage.

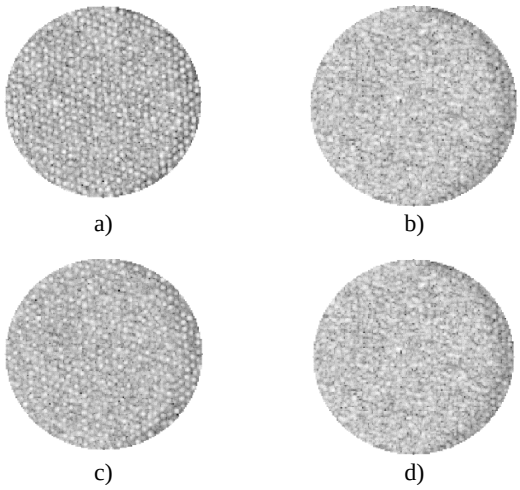

Figure 3. An example of a synthetized PolSAR image at 1 meter resolution, for different polarizations, for pine trees of 15 years old: a) HH polarization, b) HV polarization, c) VV polarization and d) VH polarization.

For the filtering method, different values for sigma were testes from which only the value of $\sigma = 0.5$ was used to evaluate the influence of the filtering stage, under the same experimental conditions, for both real and synthesized PolSAR data.

The overall accuracy (OA) is used as the evaluation parameter in this study, along with a decision level fusion with majority voting algorithm. The majority voting algorithm is used due to its capacity to allow multiple models to ensure that the best decision is made based on accuracy obtained for each stand, resulting in more accurate predictions. The decision level majority voting algorithm is designed to consider, for each individual polarization, HH, HV and VV, the corresponding label for each individual stand, label attributed in the classification

Table 1. SVM classification results for a synthetized PolSAR data using different combinations of ELBP coefficients with radii 2 and 4 for the HH, HV, VV polarizations and decision level fusion with majority voting

		CI_RD	**CI_NI**	**NI_RD**	**CI_NI_RD**
0.5m	**HH**	99.80 ± 0.73	99.49 ± 1.37	98.37 ± 2.20	98.06 ±1.46
	HV	98.80 ± 1.41	95.23 ± 3.79	89.86 ± 3.36	96.69 ± 2.25
	VV	99.60 ± 1.00	99.17 ± 1.59	98.26 ± 1.99	99.20 ± 1.52
	Majority voting	99.51 ± 1.08	99.37 ± 1.26	97.97 ± 1.96	97.97 ± 1.54
1m	**HH**	99.91 ± 0.48	100.0 ± 0.00	100.0 ± 0.00	99.31 ±1.47
	HV	99.45 ± 1.41	97.23 ± 2.35	97.37 ± 2.59	98.49 ± 1.70
	VV	99.03 ± 1.36	99.89 ± 0.56	99.60 ± 1.08	98.34 ± 1.63
	Majority voting	99.89 ± 0.56	99.94 ± 0.40	99.94 ± 0.40	98.66 ± 1.54
2m	**HH**	95.48 ± 3.22	88.40 ± 4.45	87.80 ± 4.80	86.26 ± 3.89
	HV	85.62 ± 4.84	67.86 ± 5.71	72.03 ± 4.49	79.34 ± 4.50
	VV	88.69 ± 4.84	86.14 ± 4.46	84.86 ± 4.05	85.80 ± 4.33
	Majority voting	93.34 ± 3.25	88.57 ± 4.00	85.74 ± 3.67	87.11 ± 2.77
3m	**HH**	50.22 ± 7.33	45.86 ± 6.67	53.77 ± 7.72	52.29 ± 7.41
	HV	77.17 ± 5.70	50.29 ± 7.49	52.23 ± 6.77	65.40 ± 5.15
	VV	72.57 ± 7.06	46.34 ± 8.67	52.14 ± 7.71	53.97 ± 6.83
	Majority voting	76.46 ± 6.82	51.09 ± 7.82	58.57 ± 6.67	63.77 ± 6.21
5m	**HH**	38.31 ± 6.94	45.74 ± 7.42	50.91 ± 7.29	53.09 ± 6.36
	HV	59.11 ± 6.76	59.89 ± 6.51	55.20 ± 5.32	66.06 ± 4.78
	VV	36.74 ± 7.28	35.00 ± 7.76	39.34 ± 7.31	37.89 ± 6.42
	Majority voting	51.26 ± 6.66	51.86 ± 7.33	55.37 ± 6.20	57.86 ± 6.32

Table 2. SVM classification results for a Gaussian filtered synthetized PolSAR data using different combinations of ELBP coefficients with radii 2 and 4 for the HH, HV, VV polarizations decision level fusion with majority voting

		CI_RD	CI_NI	NI_RD	CI_NI_RD
0.5m	**HH**	99.74 ± 0.82	98.86 ± 2.07	97.34 ± 2.73	98.23 ± 1.71
	HV	99.09 ± 1.40	96.26 ± 3.78	89.23 ± 3.30	97.11 ± 2.45
	VV	99.63 ± 0.97	98.54 ± 1.88	98.06 ± 1.90	99.06 ± 1.91
	Majority voting	99.63 ± 0.97	99.51 ± 1.15	97.06 ± 2.52	98.46 ± 1.69
1m	**HH**	99.71 ± 0.86	99.57 ± 1.10	100.0 ± 0.00	99.74 ± 1.00
	HV	99.14 ± 1.32	97.40 ± 2.99	95.34 ± 3.19	98.71 ± 1.43
	VV	99.66 ± 0.93	99.86 ± 0.63	99.97 ± 0.29	98.57 ± 1.44
	Majority voting	99.71 ± 0.86	99.94 ± 0.40	99.97 ± 0.29	98.89 ± 1.40
2m	**HH**	87.11 ± 5.16	83.23 ± 6.23	83.60 ± 5.47	82.14 ± 4.78
	HV	84.20 ± 4.42	65.11 ± 6.48	71.54 ± 5.63	80.14 ± 4.15
	VV	88.83 ± 3.81	82.69 ± 5.21	81.94 ± 4.77	85.91 ± 4.60
	Majority voting	92.17 ± 3.89	86.00 ± 5.71	86.26 ± 3.76	87.89 ± 3.28
3m	**HH**	45.31 ± 8.01	43.80 ± 6.84	47.49 ± 6.78	47.34 ± 5.90
	HV	79.43 ± 4.92	53.51 ± 6.52	56.11 ± 6.23	69.89 ± 4.34
	VV	67.77 ± 6.49	51.80 ± 8.31	51.97 ± 6.77	56.14 ± 6.48
	Majority voting	73.54 ± 6.49	55.83 ± 7.09	60.06 ± 6.46	66.69 ± 5.76
5m	**HH**	30.29 ± 6.95	44.86 ± 7.26	53.20 ± 7.25	50.71 ± 6.90
	HV	62.66 ± 6.19	57.46 ± 6.47	61.00 ± 6.26	65.11 ± 5.42
	VV	38.86 ± 7.13	40.20 ± 7.51	41.74 ± 6.13	43.49 ± 5.59
	Majority voting	48.20 ± 5.80	53.34 ± 6.08	58.71 ± 6.36	57.71 ± 5.71

stage. For each stand, the voting algorithm is designed to find the majority of a sequence of elements, in our case the corresponding label for a specific stand, along the three polarization images. Thus, the majority voting algorithm will return the value, in our case, the label, which occurs more often among the three polarizations. After the decision level fusion is performed, an overall accuracy is computed for all 100 iterations.

C. Results

The results in this section are presented for the synthesized PolSAR image at various resolutions, without Gaussian filtering in Table 1, followed by the filtering stage, in Table 2.

By analyzing Table 1, for all the polarizations, we can observe that the best performance for any combination of coefficients, CI, NI and RD resulted at smaller values of resolution. When the resolution of the polarimetric images decreases from 0.5 meters to 5m, the overall accuracy starts to decrease. This is due to the fact that at lower resolutions, the ELBP descriptors are not capable of extracting discriminant features from the polarimetric data. The ELBP descriptors were applied on each individual polarimetric image, on which different joint histograms, with 2 and 4 radii, were evaluated: CI_RD, CI_NI, NI_RD, respectively the joint histograms of all the descriptors, represented by CI_NI_RD. By analyzing only the 0.5-meter resolution, for all the joint histogram combinations of descriptors, we can observe that based on the type of polarization, the specific coefficients offered good classification results, placed in a certain interval. For example, for the CI_RD concatenation, the classification results oscillate at ~99% for all three polarizations. In the case of CI_NI, we can observe that the information contained in the HH polarization resulted in a better classification result, represented by a difference of ~4% compared to the HV polarization, respectively a very similar result compared to the VV polarization. When combining the NI_RD concatenation of coefficients, a decrease in classification is observed, in comparison with CI_RD and CI_NI, while the same behavior of decreasing overall accuracy results remains as in the case of CI_NI. By concatenating all three ELBP coefficients, CI_NI_RD an overall accuracy of ~98% is obtained, a value comparable to the CI_RD feature vector concatenation. For the rest of the resolutions, the classification results present the same behavior in terms of the capability of the coefficients of extracting the information from the different polarized images, due to information stored in each individual image. By taking into consideration the decision level fusion with majority voting, the best results can be considered the one given by the concatenation of CI and RD, with good overall classification results, especially for the 0.5- and 1-meter resolutions. In [6], the authors have assessed the use of a LBP and GLCM in a machine learning workflow, in which only the HV polarization was considered. The results obtained in this study are comparable with the ones presented in [6]. Taking into consideration only the 0.5-meter resolution, discussing the HV polarization, our proposed framework resulted in a performance of ~98.80% for the feature vector concatenation of CI_RD, representing an increase of ~2% compared to the GLCM method, or an increase of ~3% when a concatenation between GLCM and ELBP is used.

In Table 2, in terms of experimental results, a Gaussian filtering stage is added to study the influence of a filtering method in terms of performance. By analyzing Table 2, we can observe that the filtering method ensures an increase in performance on certain polarized images, while in other does not, in terms of classification results. This is true for all the resolutions, for any combination of ELBP descriptors, even when a decision level majority vote is considered. This means that the CI_RD ELBP joint descriptors, from Tabel 1 and 2, are effective in extracting the most valuable features, especially from the HH polarization when the 0.5 and 1 m resolutions are considered, or HV polarization when the resolution of the image is at 3 and 5 meters.

Table 3. SVM classification results for a real PolSAR data of 1m resolution, using different combinations of ELBP coefficients with radii 2 and 4 for the HH, HV, VV polarizations, without, respectively with Gaussian filtering

		CI_RD	CI_NI	NI_RD	CI_N_RD
without filtering	**HH**	88.38 ± 3.66	84.41 ± 6.34	81.22 ± 2.76	84.84 ± 3.51
	HV	85.41 ± 4.12	85.56 ± 4.98	81.59 ± 3.87	85.88 ± 3.45
	VV	89.38 ± 5.46	85.28 ± 5.55	79.84 ± 3.83	82.91 ± 4.13
	Majority voting	91.03 ± 4.59	88.78 ± 4.77	81.72 ± 3.12	85.53 ± 3.49
with filtering	**HH**	90.53 ± 3.57	87.09 ± 4.46	81.44 ± 2.58	84.66 ± 3.87
	HV	85.88 ± 4.86	84.94 ± 5.21	81.06 ± 3.71	86.94 ± 3.56
	VV	85.97 ± 4.75	82.28 ± 5.86	79.50 ± 4.20	83.63 ± 4.29
	Majority voting	90.47 ± 4.43	87.22 ± 4.42	81.66 ± 3.25	86.84 ± 3.27

In Table 3, under the same experimental evaluation, based on Fig. 1, the real PolSAR data is evaluated, considering the same joint histogram of different ELBP descriptors, for the radii 2 and 4, for each individual polarized image. As shown in Table 2, Table 3 has also the results considering the same Gaussian filtering. By analyzing Table 3, we can observe that the best performance is obtained for the concatenation of CI and RD ELBP descriptors, as discussed in the case of synthetized PolSAR data. When a filtering stage is added, the same conclusion remains for the Gaussian filtering capable of improvements in terms of performance for certain polarization images.

IV. CONCLUSIONS

In this paper we have assessed the performance of the ELBP method for the PolSAR database. An evaluation was done based on each individual HH, HV and VV polarized image on which three descriptors of the ELBP method were used to extract relevant features present at different resolutions, represented by the joint histogram concatenation of CI, NI or RD. The proposed classification framework was evaluated considering a real polarimetric image and a synthetized PolSAR database generated starting from the real data set, at various resolutions. Based on the results presented in this study we have observed that the joint multiresolution histogram of CI_RD descriptors provides the best performance in terms of overall classification, when the resolution of the image is 0.5 m or 1 m, obtained from the HH polarization, while the HV polarization returns the best results at 3m, respectively 5 m resolution. In the second part of the experiments, a Gaussian filtering stage was added. The filtering method managed to increase the performance of the classier only for several polarized images.

In this study the ELBP method, through its concatenation of its descriptors, combined with the decision level fusion with majority voting algorithm presented higher classification results compared with other state of the art methods, such as LBP and GLCM variations. Thus, the ELBP represents a valuable feature extraction method that can be applied on complex polarimetric databases due to its good multiscale feature extraction capabilities.

REFERENCES

[1] Z. Wang, X. Zeng, Z. Yan, J. Kang, and X. Sun, "AIR-PolSAR-Seg: A Large-Scale Data Set for Terrain Segmentation in Complex-Scene PolSAR Images," *IEEE Journal of Selected Topics in Applied Earth Observations and Remote Sensing*, vol. 15, pp. 3830–3841, 2022.

[2] R. Terebes, R. Malutan, M. Borda, C. Germain, L. Bombrun, and I. Ilea, "Polarimetric radar image classication using directional diffusion and descriptive statistics," *Revue Roumaine des Sciences Techniques Serie Electrotechnique et Energetique*, vol. 63, pp. 83–88, Jan. 2018.

[3] S. Guo, J. Teng, and Q. Cheng, "Exploring the Performance of Different Texture Information and Polarization Features from PolSAR Images in Urban Land Cover Classification," *Photogrammetric Engineering & Remote Sensing*, vol. 87, pp. 133–142, Feb. 2021.

[4] I. Al Saidi, M. Rziza, and J. Debayle, "Completed homogeneous LBP for remote sensing image classification," *International Journal of Remote Sensing*, vol. 44, no. 12, pp. 3815–3836, Jun. 2023.

[5] L. Zhang, "Fabric Defect Classification Based on LBP and GLCM," *Journal of Fiber Bioengineering and Informatics*, vol. 8, Mar. 2015.

[6] I. Ilea, A. Miclea, and R. Terebes, "Polarimetric Image Classification using Texture Features based on the Gray Level Co-occurrence Matrix and Local Binary Patterns," in *2023 International Symposium on Signals, Circuits and Systems (ISSCS)*, Jul. 2023, pp. 1–4.

[7] L. Liu, S. Lao, P. W. Fieguth, Y. Guo, X. Wang, and M. Pietikainen, "Median Robust Extended Local Binary Pattern for Texture Classification," *IEEE Trans. on Image Process.*, vol. 25, no. 3, pp. 1368–1381, Mar. 2016.

[8] I. Hajnsek and Y.-L. Desnos, Eds., *Polarimetric Synthetic Aperture Radar: Principles and Application*. Springer Nature, 2021.

[9] T. Ojala, M. Pietikainen, and T. Maenpaa, "Multiresolution gray-scale and rotation invariant texture classification with local binary patterns," *IEEE Trans. Pattern Anal. Machine Intell.*, vol. 24, no. 7, pp. 971–987, Jul. 2002.

[10] L. Liu, L. Zhao, Y. Long, G. Kuang, and P. Fieguth, "Extended local binary patterns for texture classification," *Image and Vision Computing*, vol. 30, no. 2, pp. 86–99, Feb. 2012.

[11] S. Bandi, M. Anbarasan, and G. Linda, "S5ELBP: Supervised SAR Image Classification using SVM from SSELBP Texture Features," presented at the 2023 International Conference on Data Science, Agents & Artificial Intelligence (ICDSAAI), Dec. 2023, pp. 1–6.

[12] I. Ilea, L. Bombrun, C. Germain, I. Champion, R. Terebes, and M. Borda, "Statistical hypothesis test for maritime pine forest SAR images classification based on the geodesic distance," in *2015 IEEE International Geoscience and Remote Sensing Symposium (IGARSS)*, Jul. 2015, pp. 3215–3218.

[13] "PolSARpro - Earth Online." Accessed: Mar. 21, 2024. [Online].Available: https://earth.esa.int/eogateway/tools/polsarpro